Front. Earth Sci. 2012, 6(3): 261–275
DOI 10.1007/s11707-012-0304-4

RESEARCH ARTICLE

Coupling hydrodynamic models with GIS for storm surge simulation: application to the Yangtze Estuary and the Hangzhou Bay, China

Liang WANG[1], Xiaodong ZHAO[2], Yongming SHEN (✉)[1]

1 State Key Laboratory of Coastal and Offshore Engineering, Dalian University of Technology, Dalian 116023, China
2 China-Japan Research Center for Geo-environmental Science, Pioneer Park of Academician, Dalian University, Dalian 116622, China

Abstract Storm surge is one of the most serious oceanic disasters. Accurate and timely numerical prediction is one of the primary measures for disaster control. Traditional storm surge models lack of accuracy and time effects. To overcome the disadvantages, in this paper, an analytical cyclone model was first added into the Finite-Volume Coastal Ocean Model (FVCOM) consisting of high resolution, flooding and drying capabilities for 3D storm surge modeling. Then, we integrated *MarineTools Pro* into a geographic information system (GIS) to supplement the storm surge model. This provided end users with a friendly modeling platform and easy access to geographically referenced data that was required for the model input and output. A temporal GIS tracking analysis module was developed to create a visual path from storm surge numerical results. It was able to track the movement of a storm in space and time. *MarineTools Pro*' capabilities could assist the comprehensive understanding of complex storm events in data visualization, spatial query, and analysis of simulative results in an objective and accurate manner. The tools developed in this study further supported the idea that the coupled system could enhance productivity by providing an efficient operating environment for accurate inversion or storm surge prediction. Finally, this coupled system was used to reconstruct the storm surge generated by Typhoon Agnes (No. 8114) and simulated typhoon induced-wind field and water elevations of Yangtze Estuary and Hangzhou Bay. The simulated results show good correlation with actual surveyed data. The simple operating interface of the coupled system is very convenient for users, who want to learn the usage of the storm surge model, especially for first-time users, which can save their modeling time greatly.

Received November 6, 2011; accepted March 10, 2012

E-mail: ymshen@dlut.edu.cn

Keywords storm surge, Finite-Volume Coastal Ocean Model (FVCOM), temporal geographic information system (GIS), Yangtze Estuary and Hangzhou Bay, Typhoon Agnes

1 Introduction

Storm surge is an abnormal rise of sea surface caused by atmospheric forces, including wind stress and atmospheric pressure associated with extra-tropical and tropical cyclones (Flather, 2001). It has a great impact on coastal regions and may cause severe damage to coastal structures and loss of human lives and properties (Madsen and Jakobsen, 2004). Yangtze Estuary and Hangzhou Bay (YE-HB) are located in the east coast of China, facing open sea. They are subjected to frequent threats from tropical cyclones, suffering massive damage from resulting strong wind, storm surge and inland flooding. These tropical cyclones are mainly generated on the ocean surface, either east of the Philippine Islands, or near Guam. According to 1949–2008 statistics, about 3.5 typhoons occurred in these areas every year which made storm surge become one of the most serious oceanic disasters in the region.

Storm surge forecasting is considered to be the best way to mitigate its damage. Surge generation by extra-tropical storms was studied in Europe (e.g., Kliem et al., 2006; Zampato et al., 2006), while it caused by hurricanes in the Gulf of Mexico and Eastern USA was studied in North America (e.g. Peng et al., 2006a, b; Weisberg and Zheng, 2008), and one by typhoons was studied in Asia and Oceania (e.g. McInnes et al., 2002; Jain et al., 2007). The forecasting methods are divided into two general categories: the empirical statistical forecasting methods (e.g., Conner et al., 1957; Harris, 1959) and the numerical prediction methods (e.g., Jelesnianski, 1966; 1967). The

former methods require a sufficiently long-term observation, so they are greatly restricted; the latter one use numerical prediction results that provide information on storm forecasts, such as forecast surface wind, pressure fields, and seawater motion in the specific study area by solving a series of complex dynamic equations. With advances in computer technology, most countries adopted these methods for forecasting storm surges. Moreover, numerical prediction is one of primary measures for storm surge disaster control. For instance, the famous SLOSH model has been widely used for two-dimensional applications (Jelesnianski et al., 1992).

Numerical experiments helped us to gain insight into storm surge mechanisms. They in turn contribute to improving storm surge theories. With the appearance of high-speed computers, numerical approximations to the governing equations have been developed. In early period, structured computational grids (generally squares) in two dimensions (vertically integrated) was used (Cao and Zhu, 2000; Dietsche et al., 2007; Hu et al., 2007). However, the 2D models may overestimate (or underestimate) bottom stress. Physically unrealistic parameterizations or other techniques of surface stress are necessary to calibrate the model. They essentially ignore the vertical flow structure that may have a significant effect on simulation (Weisberg and Zheng, 2008). Then, the 3D storm surge model was developed. It allows the inclusion of mass redistribution (the balance between the net water flux into an area and the change in water level) and the representation of more realistic shorelines and bathymetries. Research is also under way to include the influence of nonlinear interaction between astronomical tides and storm surge to reflect the obvious periodic oscillations seen in storm observations (Wang and Chai, 1989). Unstructured, finite element numerical techniques were developed for storm surge models that allowed the use of computational grids composed of unstructured triangles. These grids are easily configured to represent complex topographic and bathymetric features (e.g., irregular coastlines, rivers, inlets and barrier islands, etc.). Therefore, they can provide a very high resolution in area of interest (Chen et al., 2003;2007). The accuracy of wind field input during a tropical cyclone is crucial for the results of storm surge modeling. Some classic parametric pressure or wind models are frequently used to conveniently generate symmetric wind fields (Holland, 1980). These parametric cyclone models have demonstrated accuracy of a few feet wind fields when running past cyclones. With accurate wind fields, the 3D storm surge models are now able to fully account for the effect of the astronomical tide on the total water level. They also can forecast the potential flooding during a storm. In this study, the original Finite-Volume Coastal Ocean Model (FVCOM) model, which used the wet–dry grid point method, was revised by adding the water level change due to the atmospheric pressure field for the 3D storm surge model.

In general, the storm model data input uses a DOS operating system mode. Output data files were comprised of the plotted static images. Thus, the accurateness and time effects of storm surge prediction are greatly affected. In addition, effective analysis and visual comprehension are also obstructed (Weisberg and Zheng, 2006a, b; Guo et al., 2009; Yin et al., 2009). This is a frontier research field through combing with improving meteorological observations and modeling, accuracy of bathymetric information, computational capabilities, and hurricane warning systems can enhance national disaster plans at last (Tsanis and Gad, 2001; Castrogiovanni et al., 2005). Geographic information system (GIS) enables users to handle a large amount of data in a short time frame, and allows them to allocate more time to study the engineering tasks instead of spending excess time on preliminary tasks. Numerous efforts have been made to integrate hydrodynamic models with GIS (e. g., Tsanis and Boyle, 2001; Gemitzi and Tolikas , 2004; Naoum et al., 2005; Ng et al., 2009). Such integrations provide not only efficient modeling pre-processing and post-processing, but also the system with spatial data management, analysis, and visualization functionalities (Ng et al., 2009). The paper attempted to establish the integration of a symmetric storm-induced wind and pressure field with a background, finite volume ocean model and GIS functionality. We integrated all of the modeling process into the same environment in order to fully use the advantages of both GIS and numerical modeling, including mesh calculation, model parameter selection and setting, model computation, and the final results visualization. The system can complete and improve the operability of model application and the decision-making efficiency. Thus, we solved the problems associated with traditional storm surge numerical method including issues with data collection, visualization, spatial query, and analysis of simulative results. As a synthetic measure and inversion/prediction for storm-surge disaster control, the system combines GIS with storm-surge numerical model felicitously, and provides well operating environment for visualization, spatial query and analysis of simulative results.

Using the example of the storm surge which was induced by No. 8114 Typhoon Agnes crossing the YE-HB, the paper discusses the essential integrated technology in which we embedded ComGIS DLL (*MarineTools Pro*) of the storm surge numerical model inside the ArcGIS implemental software (Merkel et al., 2008; Tsanis and Gad, 2001; Ng et al., 2009). The development of the integrated system of storm surge numerical prediction supported by GIS is also included. The ways and specialties of the Desktop GIS development are summed up. The integrated methods of GIS and professional applied model are analyzed. The system shows seamless integration for GIS and all phases of the numerical model, including model preprocessing, model computation, model post-processing, and results visualization. For example, the

Digital elevation model was utilized to make water landforms to generate the difference-grid data automatically. The spatial database technology of GIS was then applied to realize chart show and allow spatial query on information, such as water depth, typhoon route and tidal level. It also enabled to correlate with prediction of storm surge. GIS visualization technology was applied to simulate coastal dynamic environments (such as flow field, storm surge water accretion distribution) and their transformation process in typhoon-affected regions. The integrated model was used to reproduce the storm surge generated by Typhoon Agnes (No. 8114), and simulate typhoon-induced wind field and water elevations of YE-HB. The results show that the system is good, easy to operate. It can improve the efficiency of decision-making for the storm surge numerical model.

The paper is organized as follows. In Sect. 2, the numerical model coupled in system is described. The model consists of a symmetric storm-induced wind model and a revised FVCOM hydrodynamic model that involves the effect of the atmospheric pressure change. In Sect. 3, the method of coupling GIS with hydrological modeling is presented. Then, the process of YE-HB storm surge induced by Typhoon Agnes (No. 8114) is simulated to validate the developed *MarineTools Pro*, and the simulation results are compared with the observed data. The conclusions are outlined in Sect. 4.

2 Integrated system design

2.1 Parametric and analytical cyclone model

The accuracy of the atmospheric pressure and wind field during a tropical cyclone input is crucial for storm surge modeling. However, we often have limited information, such as cyclone position, pressure drop, maximum wind speed, and radius to maximum wind speed. The advantages of parametric and analytical cyclone models are that they can reproduce the wind and pressure distribution characteristics of a tropical cyclone with limited information. The cyclone model can also be used to study the sensitivity of each stage to changes of track, central atmospheric pressure, radius of maximum wind velocity, and other parameters (Hubbert et al., 1991; Jakobsen and Madsen, 2004; Guo et al., 2009). The analytical air pressure and velocity distributions require very limited information about the cyclone in terms of the radius to the maximum wind, the maximum wind speed, and the pressure drop. Analytical expressions of the tangential and radial cyclone velocity distributions are derived from the governing momentum equations. The shape parameter of the cyclone air pressure and wind field can be determined on the basis of empirical relationships between the maximum wind speed and the pressure drop. Together with information about the cyclone position, it is then possible to simulate the induced storm surge using a hydrodynamic model. In this model, the derived analytical wind speed distribution is transferred to shear stress and the atmospheric pressure field which is added to hydrodynamic model for the water level change. The Jelesnianski model was selected to simulate the wind field and atmospheric pressure (Jelesnianski, 1966). The model equations are as follows:

$$P_r = \begin{cases} P_0 + \dfrac{1}{4}(P_\infty - P_0)\left(\dfrac{r}{R}\right)^3, & (0 < r \leqslant R), \\ P_\infty - \dfrac{3}{4}(P_\infty - P_0)\dfrac{R}{r}, & (r > R), \end{cases} \tag{1}$$

$$W_r = \begin{cases} W_R\left(\dfrac{r}{R}\right)^{1+\beta}(A\bar{i} + B\bar{j})\dfrac{1}{r} + \dfrac{r}{r+R}(V_{0x}\bar{i} + V_{0y}\bar{j}), \\ \qquad\qquad (0 < r \leqslant R), \\ W_R\left(\dfrac{R}{r}\right)^{\beta}(A\bar{i} + B\bar{j})\dfrac{1}{r} + \dfrac{R}{r+R}(V_{0x}\bar{i} + V_{0y}\bar{j}), \\ \qquad\qquad (r > R), \end{cases} \tag{2}$$

where P_r and W_r: the surface air pressure and wind vector at a radial distance r from the cyclonic center, respectively; R: radius of maximum wind velocity; r: the distance from the calculating point to the center of typhoon; V_{0x}: x-component moving velocity of typhoon; V_{0y}: y-component moving velocity of typhoon; $\bar{i}$ and $\bar{j}$ represent x and y components, respectively; W_R: maximum wind velocity at the radius R, which is calculated by the wind-pressure equation of Atkinson and Holliday (1977); $A = -[(x-x_c)\sin\theta + (y-y_c)\cos\theta]$; $B = [(x-x_c)\cos\theta - (y-y_c)\sin\theta]$; (x, y): the coordinate of calculating point; (x_c, y_c): the coordinate of the typhoon center; θ: the flow angle (in calculation, when $r \leqslant R$, θ is 10°; $r \geqslant 1.2R$, θ is 25°, and when $R < r < 1.2$, θ value is a linear interpolation between them); P_0: atmospheric pressure at the center of the typhoon; P_∞: the peripheral atmospheric pressure; β: the attenuation coefficient of wind in distance. In actual observation, compared with the central low pressure, the maximum wind speed observation is more difficult, hence the error is greater. Atkinson and Holliday (1977) studied a large number of tropical cyclones in the Pacific North-west and constructed a relationship between wind speeds calculated for a pressure and maximum wind speed, the formal expression is as follows:

$$W_R = 3.44(P_\infty - P_0)^{0.644}, \tag{3}$$

where W_R and P_∞, P_0 units are m/s and hPa, respectively. Powell and Houston (1998) considered that the above relationship was also applicable to estimate the maximum wind speed in other tropical storm regions. The gradient wind needs to be adjusted to the 10 m height surface wind

speed that multiplied by the coefficient 0.8, corresponds to parameter wind. The result is equivalent to the 8–10 min average wind speed. Hurricane wind stresses (τ_{sx} and τ_{sy}) acting on the surface boundary are computed using conventional bulk formula:

$$\tau_{sx} = 0.8C_s\rho_s W_{rx}\sqrt{W_{rx}^2 + W_{ry}^2}, \quad (4)$$

$$\tau_{sy} = 0.8C_s\rho_s W_{ry}\sqrt{W_{rx}^2 + W_{ry}^2}. \quad (5)$$

where ρ_{air} is air density, C_{wd} is drag coefficient related to boundary wind velocity W_r, W_{rx} and W_{ry} are wind velocity components.

2.2 Storm surge model

Major destructive storm surges tend to occur when extreme storm winds and surface pressure gradient forces act over extensive regions of shallow water. The air-sea momentum flux is a key surface force in storm surge modeling. It is because that the wind stress term is divided by the total depth, the surface pressure gradient force and wind force terms in the governing equations. Thus, the storm surges increase rapidly over shallower water (e.g., Flather, 2001). Pressure force and wind stress are crucial factors which determine model performance. The air-water drag and bottom friction are particularly important in areas of inundation or coastal wetlands. It is the wind stress that generates most of the total cyclone-induced storm surge in coastal seas. Storm surge fluctuates significantly in addition to long-wave effect caused by the storm disturbance, but there is a coupling of astronomical tide and storm surge. The fluctuations in the tidal cycle are primarily caused by the coupling of astronomical tide and storm surge. The strength of the fluctuations depends on the relative direction of movement, tidal drop range, and the size of water rise, so that the extreme water rises do not appear when there is a high tide. In this study, we only investigated the effects of the conventional long wave storm surge. Short surface waves were not included.

In this paper, an analytical cyclone model was added into the time-dependent, FVCOM is a 3D free surface primitive equation model (Chen et al., 2003), to simulate tide and 3D storm surge. FVCOM has been tested against other well-established models. It was widely used in studies of coastal ocean circulation (e.g., Chen et al., 2007; Huang et al., 2008; Li et al., 2008). It incorporates the Mellor and Yamada (1982) level 2.5 turbulence closure sub-model modified by Galperin et al. (1988) and the Smagorinsky (1963) formulation to parameterize flow-dependent vertical and horizontal mixing coefficients, respectively. σ-coordinate transformation is used in the vertical direction to accommodate irregular bathymetry, to accurately represent coastlines and bathymetry, so we can apply appropriate boundary conditions and arbitrarily choose mesh resolutions (regardless of the vertical coordinate used). Emphasis can therefore be in the coastal areas where coastline sand bathymetries can be quite complex, and the most severe storm surges tend to occur. FVCOM solves the primitive equations by using a flux calculation integrated over each model grid control volume. It ensures mass, momentum, energy, salt, and heat conservation in the individual control volumes and over the entire computational domain. Similar to the Princeton Ocean Model (POM) of Blumberg and Mellor (1987), a mode-splitting method with external and internal mode time steps, which accommodate the faster and slower barotropic and baroclinic responses respectively, is used for computational efficiency. FVCOM also includes provision for flooding and drying, which is a critical element of storm surge simulation (e.g., Hubbert and McInnes, 1999).

On the coupling of the storm surge and astronomical tide, it is necessary to consider the role of astronomical tide, along with the typhoon in the computational domain and the deep seawater open boundaries. The typhoon affects the seawater body through the provision of air pressure and wind field in the typhoon model calculation, in accordance with the static pressure hypothesis and free surface boundary conditions in the computational domain and the open boundary. The astronomical tide level is taken as the main driving force through the astronomical tidal constituent of the boundary conditions. But origin FVCOM does not provide the typhoon air pressure and wind field simulation model. It needs to establish its own corresponding typhoon model to couple typhoon-induced pressure and wind press into an FVCOM. We added the parametric and analytical cyclone model in Sect. 2.1 for the wind and pressure distributions of a prototypical tropic cyclone (see Fig. 1).

With Boussinesq and hydrostatic approximations, the primitive equations of momentum and mass conservation include the atmospheric pressure term, which make bottom-layer return currents produce a shoreward bottom stress that adds to the wind stress (enhancing surge). The complex opposing effects due to waves depend strongly on local bathymetry (Resio and Westerink, 2008). Furthermore, the effect is partially accounted for using sea-state strong winds correction. With regard to coastal wave setup, this term is relatively less important in wide continental shelves (McInnes et al., 2002; 2009). Integrating equation $\frac{\partial P}{\partial z} = -\rho g$ from the sea-bed to the sea-surface, we can get

$$P = P_{atm} + \rho g(\zeta - z), \quad (6)$$

where P_{atm} is the atmospheric pressure change, ζ is the sea-surface elevation. In the above equation, normal atmospheric pressure becomes the typhoon-induced pressure. It

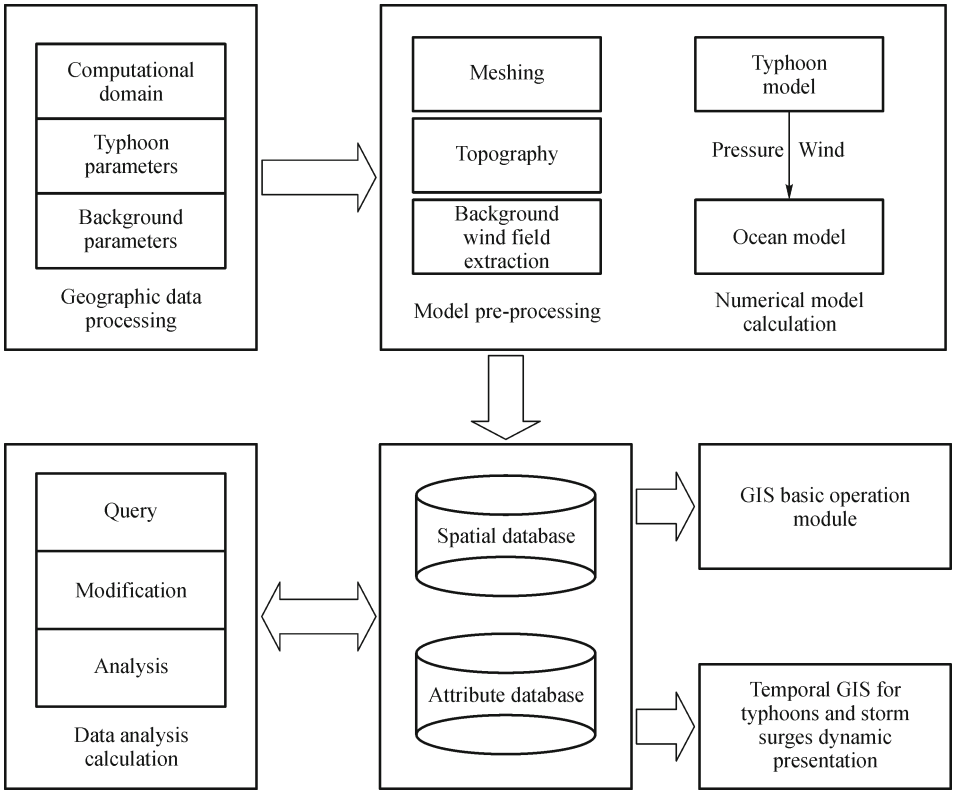

Fig. 1 General logical structure of storm surges system

forms a special low-pressure state in the typhoon center. We added the pressure item into the FVCOM. The following stretching σ-coordinate is introduced in the vertical direction. All the equations will include the new variable σ instead of z. Equation transformation detail can be seen in literature (Chen et al., 2003; 2007). With hydrostatic assumption, we ignored the vertical acceleration, z direction of the momentum equation.

$\frac{\partial P}{\partial z} = -\rho g$ becomes $\frac{1}{D}\frac{\partial P}{\partial \sigma} = -\rho g$ in σ-coordinate system, in which D is the total water column depth, and integrals to this formula. We note, $P|_{\sigma=0} = P_{\text{atm}}$ and there is: $P = -D\rho g\sigma + P_{\text{atm}} = -\rho g(z-\zeta) + P_{\text{atm}}$, then we will get

$$-\frac{1}{\rho}\frac{\partial P}{\partial x} = \frac{1}{\rho}\frac{\partial\left(\rho g(z-\zeta) - P_{\text{atm}}\right)}{\partial x} = g\frac{\partial(z-\zeta)}{\partial x} - \frac{1}{\rho}\frac{P_{\text{atm}}}{\partial x} = -g\frac{\partial \zeta}{\partial x} - \frac{1}{\rho}\frac{P_{\text{atm}}}{\partial x}. \quad (7)$$

We also used finite volume discrete method to deal with the new term in the above equation (Chen et al., 2006). The surface and bottom boundary conditions for momentum are (τ_{sx},τ_{sy}) and (τ_{bx},τ_{by}), which are the typhoon-induced wind stress and bottom stress components, respectively. Wind stress is computed from:

$$\overline{\tau} = C_{\text{d}}\rho_{\text{air}}|\vec{V_W}|\vec{V_W}, \quad (8)$$

where C_{d}, a drag coefficient dependent on wind speed $\vec{V_W}$, is given by Large and Pond (1981)

$$C_{\text{d}} \times 10^3 = \begin{cases} 1.2, & |\vec{V_W}| \geqslant 11.0\text{ms}^{-1}, \\ 0.49 + 0.065|\vec{V_W}|, & 11.0\text{ms}^{-1} \leqslant |\vec{V_W}| \leqslant 25.0\text{ms}^{-1}, \\ 0.49 + 0.065 \times 25, & |\vec{V_W}| \geqslant 25.0\text{ms}^{-1}. \end{cases} \quad (9)$$

First, we simulated astronomical tide. A few tidal cycles were calculated in order that the simulation would stabilize. The calculated tide time and tide level should agree with real reported values. Then, we introduced typhoon parameters to calculate with the tidal wave at the same time, produced a calculated coupling effect with the typhoon and tide. On the boundaries, linear addition of these two terms is permissible. Because the boundaries are far off the coast and the water there is deep. Result corresponding to this value minus the calculated astronomical tide, which produces the storm surge values with astronomical tide and storm surge in coupling.

2.3 GIS-based integrated system

The GIS-based integrated system was carried out using the latest version of ArcGIS 10 (ESRI). ArcGIS 10 provides several alternative methods to extend GIS functions, such as the Python-based scripting approach and the ArcObjects approach. The new Desktop add-in model is easily developed and shared among users, as it does not require installation programs or Component Object Model (COM) registration. The professional add-in is added to a system by simply copying it to a well-known folder and removed by deleting them from this folder. The most difficult and critical issue is that the data interfaces between the surge model and GIS, because information of the user interacts with the system in every way through the interface, its design is of vital importance to the productive use of the system. In essence, to the user, the interface is a system (Frank, 1993; Gould, 1993). We have cleverly solved this problem with the NetCDF file, which is a data format and library designed to store multidimensional arrays of scientific data. It is widely used in the atmospheric sciences and oceanography. With the improved *Multidimension Tools* toolbox, we make GIS create raster layers, feature layers, and table views from NetCDF data, or convert feature, raster, and table data to NetCDF.

In the paper, we integrated the surge model to the ArcGIS desktop with the Com GIS technique in order to form the integration system that implements GIS for all phases of the storm surge model, including model preprocessing, model computation, model post-processing, and numerical result's visualization, GIS tracking analysis module was also developed. It is easy to operate and improve the efficiency of decision-making. It is also an inversion and prediction system for typhoon wind and tidal wave, which is applied to investigate the hydrodynamic responses to the frequent threats from typhoon-induced storm surge.

Figure 2 shows a schematic sketch of *MarineTools Pro* add-in, in which an Interface Data Model (IDM1, IDM2 and IDM3) was used to act as a bridge between the GIS spatial model and the storm surge model. The GIS and surge model are kept as separate entities and linked by input-output manipulation through pre-processing and post-processing within the GIS menu-driven graphic user interface.

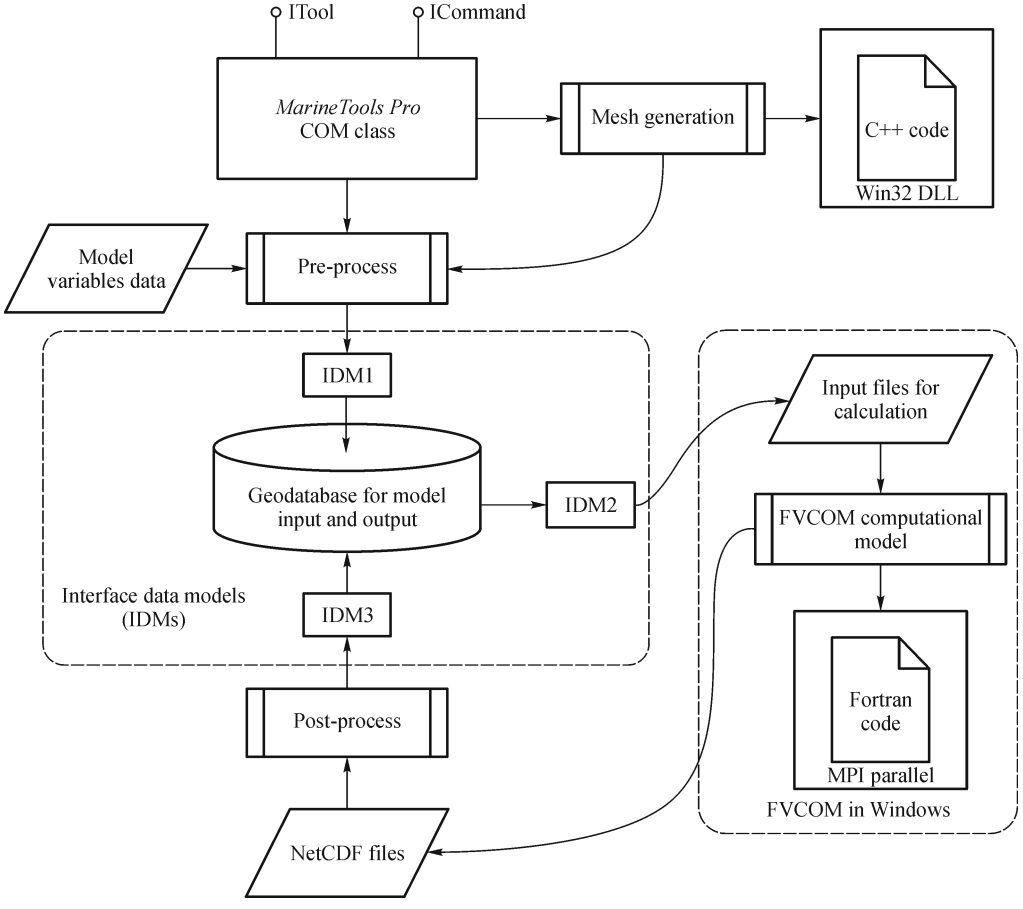

Fig. 2 A schematic sketch of *MarineTools Pro* data model. The interface data model used Geodatabase within ArcGIS providing easy translation of FVCOM input and output data

2.3.1 Model of pre-processing

The pre-processing component was developed for retrieval, manipulation, editing and displaying of geographical data and bathymetry in the study area, including the configuration and refinement of the mesh grid, the export of the model input data through the GIS interface (Fig. 2). The system used the part of the East Asian and Northwest Pacific region as a background base map. Required data include: a graphical computing area polygon selected in the GIS map, the background wind field file, measured bathymetry in the target region, inflow and outflow for source elements, initial conditions and boundary conditions of tidal elevation, and mesh grid conflguration. Processing in temporal GIS of typhoon input parameters are as follows: typhoon center, center of the lowest pressure, typhoon speed, and maximum wind radius. Input and output of source file are all forms of running processes. They are displayed as NetCDF interface in GIS. As an independent system, the source code can be rewritten as a console application, so that the surge model for the program can be integrated into the application system in the form of call function.

2.3.2 Model of post-processing

The main intention of the post-processing component is to take the model output data and display them in the forms of spatial layer (vector or raster), time series, and profile. A module was written to convert the output text file into Database File (DBF) format (Fig. 2). We then designed our data structure. Table 1 shows the structure of the typhoon data for surge model results. The retrieval DBF format data made the system more efficient than text format data. Any object had three basic elements in a certain geography space-time coordinate, space, time and attribute. Dynamic display is the manner that considers the time in the process of object's changing and simulates the dynamic situation following the time in order to represent the essence and change of the object quickly and smoothly. Function of temporal GIS which is dynamic displayed provides a geographical analysis platform environment. The application areas are extended. It makes the observed targets visual in the time and space, traditional planar and static state maps dynamic and visual. Therefore, the function of displaying space-time data was enhanced in GIS. In this paper, the dynamic display of the typhoon route and enlargement of the build distribution were carried out by position dynamic change model.

We have developed the interface of the storm surge model and GIS, making GIS use of *Tracking Analyst* to express the results of the model simulation result. We developed GIS add-in model that extended the display function for typhoon space-time data, such as the typhoon wind field and other typhoon parameters (i.e., typhoon center and maximum radius), and increased the analysis function of these space-time data in ArcGIS. With ArcGIS *Tracking Analyst*, we can visualize typhoon path change over time, symbolize the age of typhoon data by color, size, or shape, group and symbolize data by entity or track, interactively play back time-based typhoon data, analyze historical analysis, which enables users to create time series visualizations, If we can get information from connections to the ArcIMS Tracking Server, users can analyze information relative to time and location or real-time typhoon data, and it can create animation files for AVI output too. ArcGIS *Tracking Analyst* can display surge model results with point layer (typhoon center), polyline layer (wind field induced by typhoon), polygon layer (maximum radius), and typhoon tracks. Then, ArcGIS can create a visible path, or track, showing movement through space and time of the phenomena that users are analyzing. We are able to view complex time series and spatial patterns in an integrated storm surge and GIS system, e.g., users can record, play back, and conduct temporal analysis including data clock charting and

Table 1 Structure of the typhoon data for surge model results

No.	Field name	Field description	Type	Length	Key	Remarks (Null)
1	ID	Index	Integer		Y	N
2	PassTime	Pass time	Date		N	N
3	UserID	User	Integer		N	Y
4	Error	Error info	String		N	Y
5	Longitude	Longitude	Double	Default	N	Y
6	Latitude	Latitude	Double	Default	N	Y
7	EVector	East component of wind vector	Double	Default	N	Y
8	NVector	North component of wind vector	Double	Default	N	Y
9	Ucenter	East component of center speed	Double	Default	N	Y
10	Vcenter	North component of center speed	Double	Default	N	Y
11	R0	Maximum speed radius	Double	Default	N	Y
12	Pressure	Center pressure	Double	Default	N	Y

temporal offset. Moreover, monitoring and analysis actions are available, such as highlight, suppress and filter. Existing temporal typhoon data can be set with future time windows (for mission planning) or past time windows (for historical data).

3 Case study

In Northwest Pacific coastal countries, China was frequently hit by typhoons, with up to 34% making landfall. According to 1949–2008 statistics, about five typhoons which caused more than 100 cm of storm surge occurred in the China coastal area every year. The YE-HB zone located in the East of China faced frequent threats from tropical cyclones. It suffered massive damage from strong wind, storm surge and inland flooding. Yangtze River, the longest in China, has the largest runoff. Yangtze River Estuary is a typical allusion islands branching type tidal estuary which is affected by the strong runoff and tidal current power. Hangzhou Bay has one of the world's largest tidal bores, containing lots of small islands (Fig. 3). The coastlines of computational area are very complex. Typhoon Agnes was initially formed about 600 km west-north-west of Guam on 25/08/1981, and rapidly developed into a tropical storm on 27/08/1981, moving west-north-west toward Eastern China Sea on 29/08/1981 (GMT + 8, Beijing Mean Time). In the subsequent days, when the typhoon moved toward the estuary mouth, lower atmospheric pressure in the typhoon center caused a relatively high-water elevation in adjacent areas, and strong surface wind pushed a huge volume of seawater into the estuary. Typhoon Agnes greatly influenced the hydrodynamics and caused a significant rise of water level, especially in Hangzhou Bay, which led to an extremely high recorded water level.

A real-time storm surge model was performed to reproduce the hydrodynamic response to Typhoon Agnes, tracking position and central pressure of Typhoon Agnes for the period of 2:00 30/08/1981 to 2:00 02/09/1981 are given (every 6 h). The pressure and wind fields were treated as external forces on the water surface boundary in the model. A set of model input files was generated following the processing of the integrated model system based on geographical and other data. Model simulation was then carried out using the model input files. The model generated an interface NetCDF file after the simulation was completed. The NetCDF file was further converted to GIS DBF files for efficient retrieval. In this study, the computational domain covers the YE-HB and adjacent shelf, having an extensive range of 116°E –138°E in longitude, and 21°N – 41°N in latitude. We locally refined the concerned regions with small triangular meshes. Figure 4(a) provides a comprehensive overview on the model input setup for the simulation, including water depth raster layer, element sources, meshes grid configuration, and typhoon increasing elevation. The water depth raster layer was generated from interpolation of the model input bathymetry point layer. The horizontal triangular grid has 56439 nodes and 107931 elements, with the maximum 10000 m grid size in open boundary and the minimum 500 m grid size near the shoreline of the Zhoushan Islands (Fig. 4(b)), 10 sigma levels are used in the vertical. The topography in the computational domain was linearly interpolated to the gird calculation points. Atmospheric forcing, wind stress, and pressure perturbation were externally calculated using cyclonic models and imposed on the model system via surface boundary condition. At the sea bottom, the bottom shear stress is induced by the bottom boundary friction. The elevation clamped open boundary condition was provided along the time-dependent water elevations consisting of the seven main tidal constituents M2,S2,N2,K2,K1,O1,P1 (calculated by the Global Ocean Tide Models) and typhoon generated water surface variations on the deep sea off the coast. On the land side of the model domain, runoff from Qiantang River and Yangtze River was prescribed by maximum values in the model according to the long-term field observation during the storm event. The external time step was 10 s. The ratio of internal time step to external time step was 10. Half a day (12 h) slowly ramping was taken as the starting point of three days (72 h) Typhoon Agnes storm surge simulation. A point spatial layer of current velocity for the surface layer, overlaying a raster of depth, was generated at simulation time interval. The simulation shows that the direction of the current

Table 2 Comparison of the observed and simulated values

Gauge station	Time of the highest tide	The highest sea level/m		Error/m	Typhoon No.
		Observed	Simulated		
Changtu	23:00 9/1/1981	2.45	2.31	−0.14	
Daji	00:00 9/2/1981	2.99	2.63	−0.36	
Ganpu	02:00 9/2/1981	4.28	4.49	0.21	
Tanxu	02:00 9/2/1981	4.14	4.03	−0.11	8114
Wusong	01:00 9/1/1981	2.72	2.76	0.04	
Zhapu	02:00 9/2/1981	3.66	3.54	−0.12	
Zhenhai	01:00 9/1/1981	2.12	2.11	−0.01	

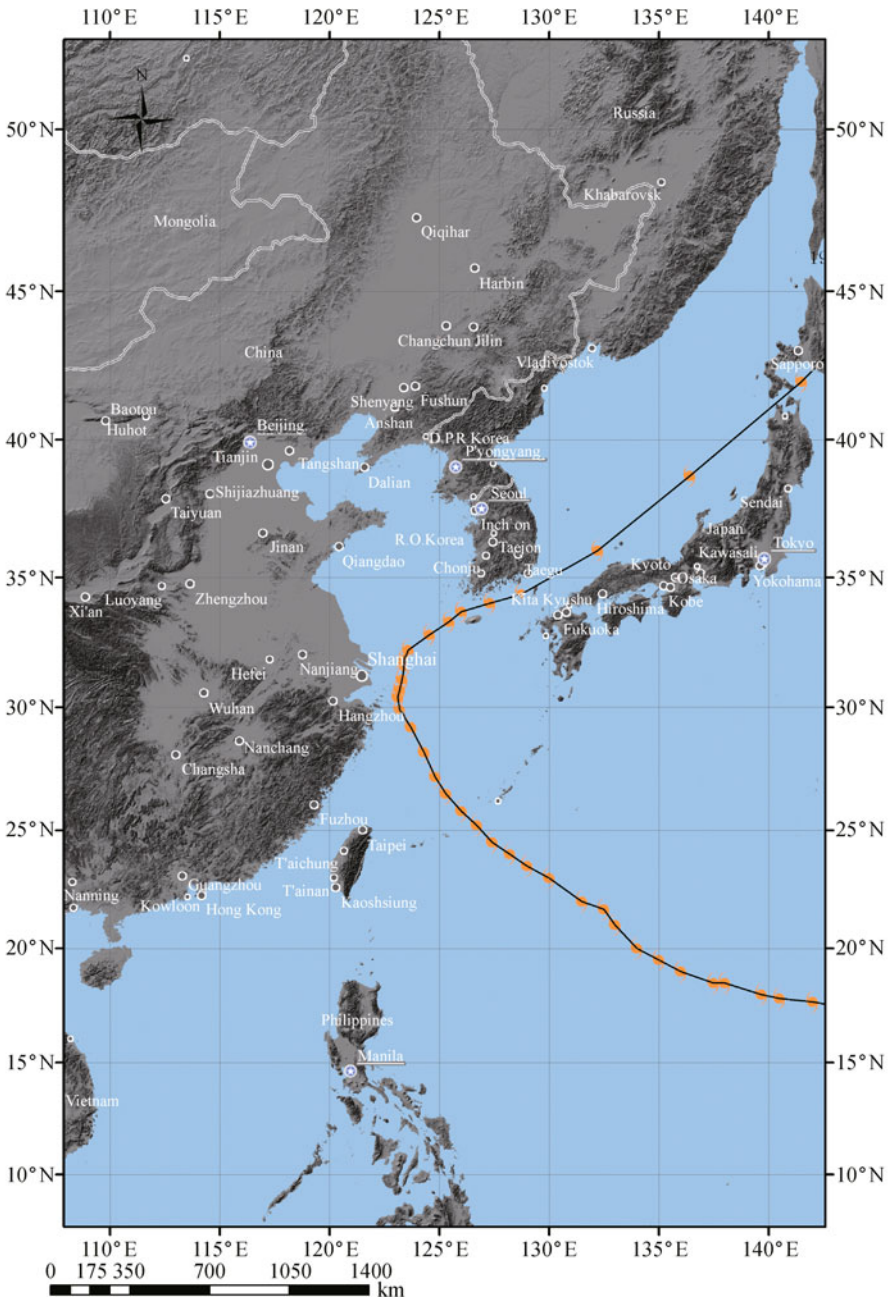

Fig. 3 Case study region: East China Sea

corresponded well with the ebbing tide and the current was moving away from the coastal region toward the sea. The entire seawater elevation field was represented by a graduated color scale, with the lightest shade for the lowest value, and the darkest shade for the highest value. The level was relatively low at the shore area and increased gradually toward the open sea.

To examine the integrated model system ability, it was initially applied to reproduce the storm surge generated by Typhoon Agnes, during which field observations were carried out and the calculated surface wind field and water elevations at two stations (Daji and Tanxu) were compared with available field measurements for validating the model. Figure 5 shows the comparisons of calculated and observed wind speed and direction at both Daji and Tanxu stations. The starting time was at 00:00 on 30/08/1981 (Beijing Mean Time), which applied to time abscissa in both Figs. 5 and 6. It can be seen from Fig. 5 that the simulated wind speed at both stations was slightly smaller than the field measurements during the early stage of cyclonic development, with an averaged difference of 2.03 m/s. This discrepancy existed probably due to the fact that the symmetric cyclonic model did not reflect the asymmetrical shape of a near-shore typhoon. The predicted

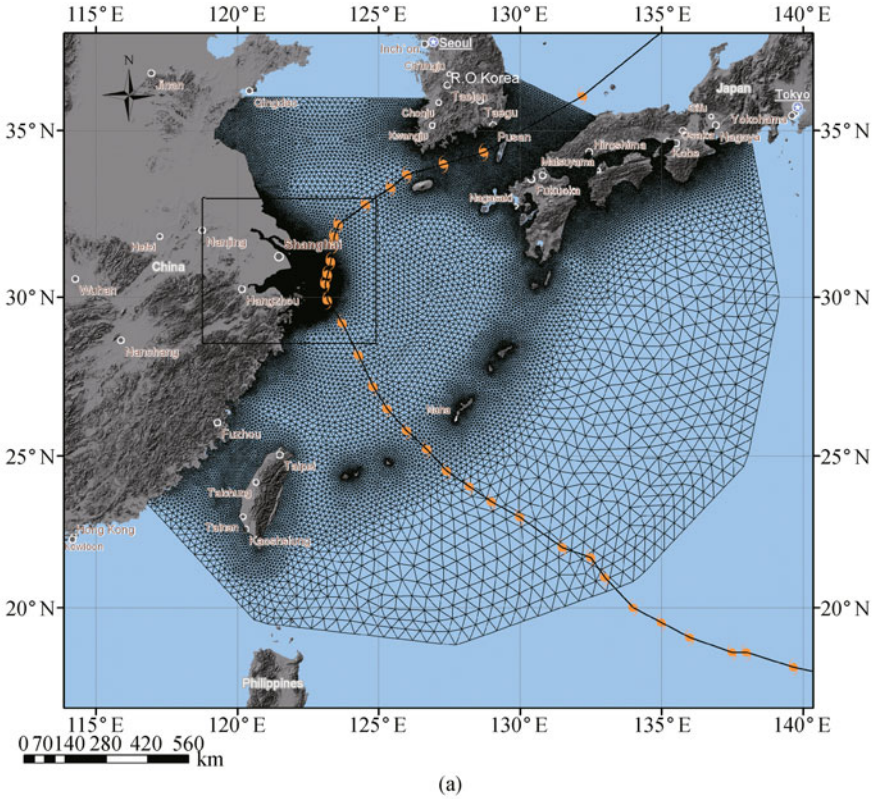

Fig. 4 (a) Map of the East China Sea, including Typhoon Agnes (No. 8114)'s track. The box indicates the zoom shown below. (b) Map of the YE-HB region most affected by Typhoon Agnes, showing names of coastal features (e.g., cities, provincial boundaries and gauge stations)

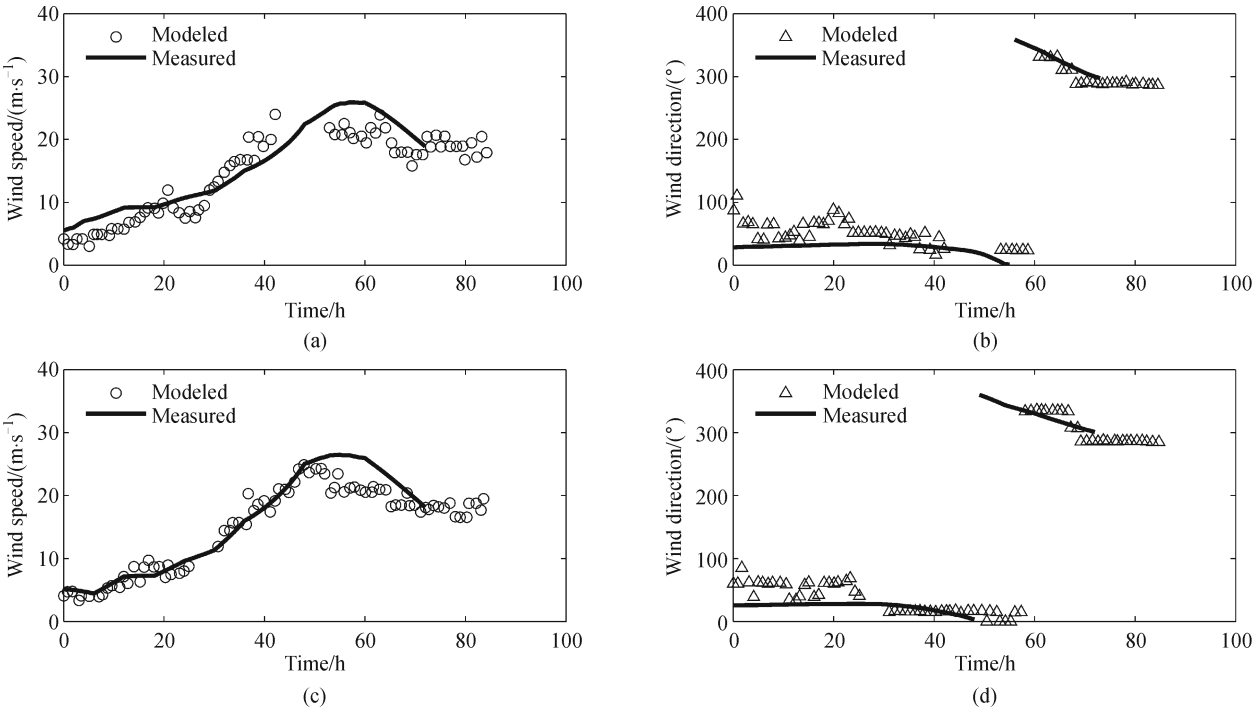

Fig. 5 Validation of Typhoon Agnes wind field. (a) and (b) represent Daji station; (c) and (d) represent Tanxu station

wind directions in these two stations agreed well with the measurements, with the averaged difference being about 5.6° at the Daji station and 8.5° at the Tanxu station, respectively. The simulated water elevations were compared with the observed data in Figs. 6 (a) and (c). It shows that the simulated elevation of high water was slightly

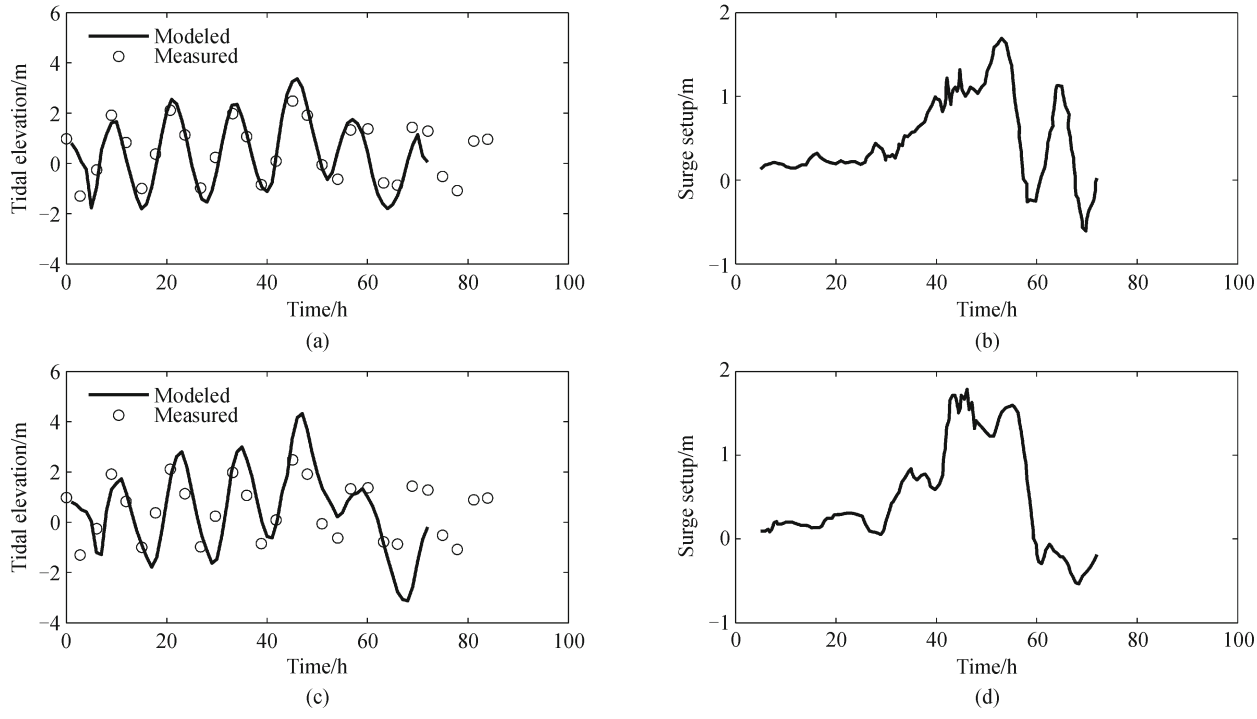

Fig. 6 Validation of Typhoon Agnes water elevation and surge setup. (a) and (b) represent Daji station; (c) and (d) represent Tanxu station

smaller than field measurements, which might be ascribed to the discrepancy of calculated wind field. The normalized root mean square deviations between numerically calculated values and the observed values were 5.31% and 4.34% at Daji and Tanxu stations, respectively. A series of time dependent surge setup, the difference of water elevations in the storm surge modeling and those in purely astronomical tide simulation, are used to represent the impact of a typhoon-generated storm. Figures 6 (b) and (d) displays the simulated surge setup at both the Daji and Tanxu stations. The trend of the surge setup development at the two stations was similar. Table 2 shows the comparison of the observed and simulated data at whole time point. The surge setup increased steadily during the early stage (0–50 h) of typhoon development, and reached the peak (about 1.0 m higher than astronomical tide) on the 22nd h. (at 22:00 on 31/08/1981). The surge setup then quickly decreased when the wind direction changed from

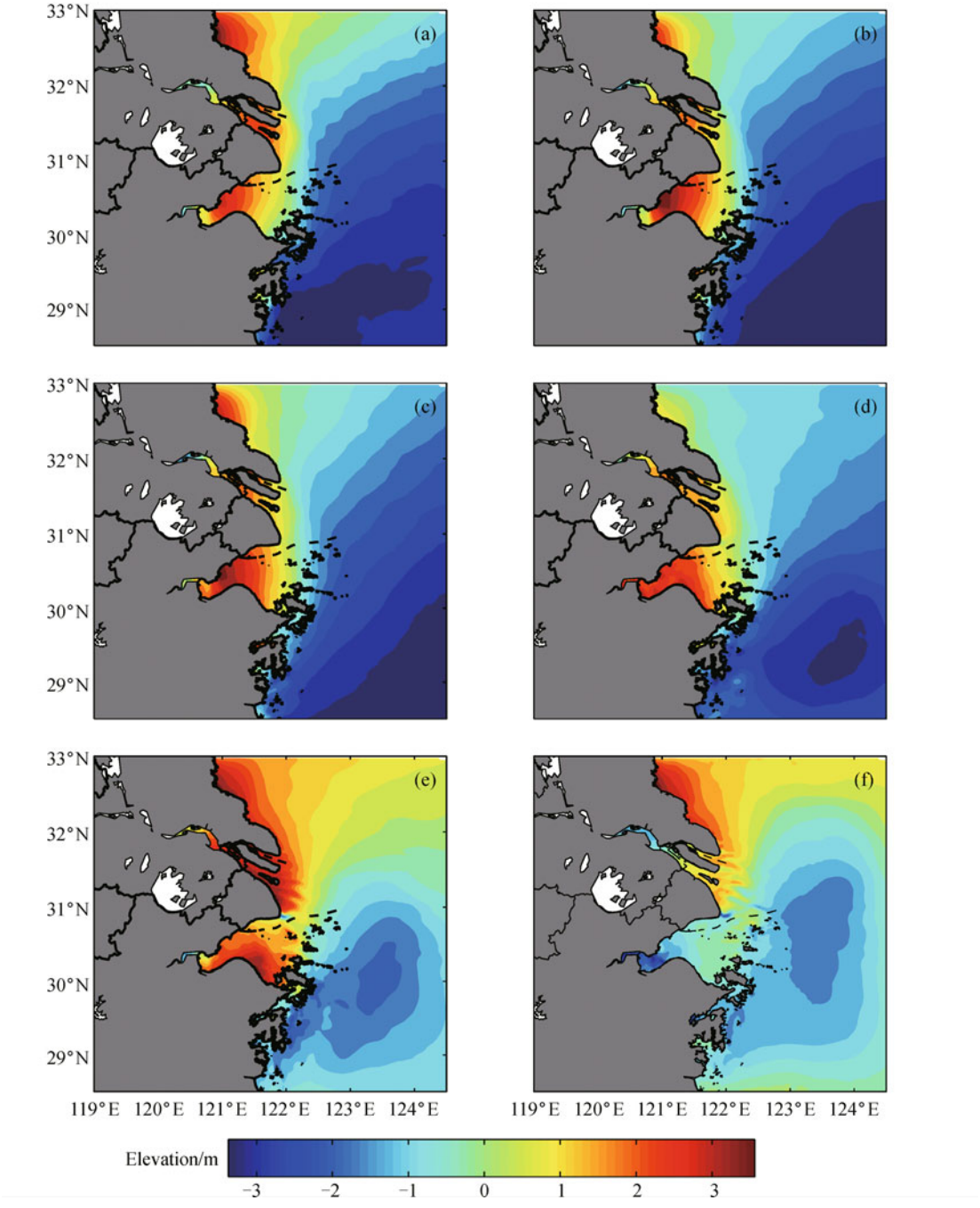

Fig. 7 Model simulated sea level elevation from 08/30/12:00 (a) to 09/20/00:00 (f) (GMT + 8 Beijing Mean Time) in 12-hourly snapshots

northeast to northwest after 54 h. In general, the northeast wind pushed water into Hangzhou Bay, causing higher water elevation; while the north-west wind dragged water out of Hangzhou Bay, causing lower water elevation. The results indicated that the typhoon induced external force, especially wind stress, which had significant impact on the water elevation. Figure 7 shows sea levels elevated everywhere along the coast to the north of the eye, particularly in the YE-HB. To the south of the eye and within Xiangshan Harbor estuary (in Zhenjiang Province), sea level was set down. Sea level was set down inside Hangzhou Bay when the storm passed.

4 Summary

GIS is distinguished for geographic referencing. It helps to relate spatial entities. GIS software has been developed with specialized software modules. This trend is a reflection of the maturing of GIS as an industry and the increasing demand by users for tailor-made and streamlined solutions to specific application areas.

In this study, the description of storm surge model by revising FVCOM model, which was added with pressure and wind items introduced by symmetric typhoon model, had been given. Then, the 3D surge model was integrated to the ArcGIS platform with COM components. An interaction among system components using GIS specialized software modules through a typhoon event across YE-HB case was presented in the paper. The implementation process and the model running results had been presented. This GIS specialized software module promoted the successful and accurate application of sophisticated storm surge simulation through a simple and straightforward graphic user interface. GIS was coupled with surge model for input viewing and editing, pre-processing, mesh grid generation and result interpretation. The GIS-model integrated system distinguished itself from others with its ability through facilitating FVCOM unstructured grid, using COM-GIS approach and developing with GIS data format to express the numerical model data structure. The application of GIS interface in defining and interpreting model input and output information tremendously improved the FVCOM model, and the system promoted better decision-making in coastal environment management. It also enhanced the usage of 3D storm surge model through a simple and easy-to-use graphic user interface (Fig. 8). The user-friendliness of this application reduced

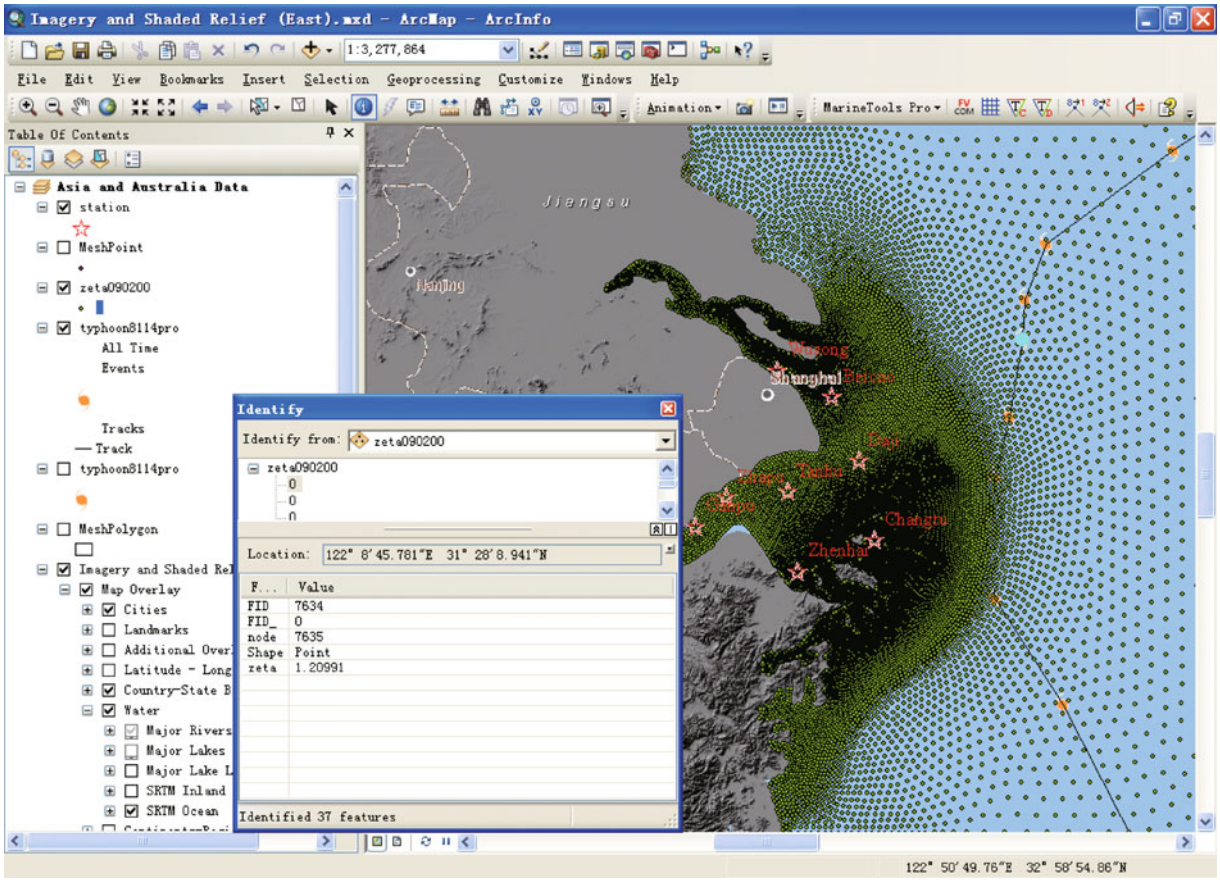

Fig. 8 Display of a spatial point layer model output of sea elevation for simulation time 9/2/1981 00:00:00 pm in the GIS mapping window and *Identify* tool displays the node ID 16280 at the selected typhoon time point

the time needed to comprehend the usage of the model, particularly for first-time users. Furthermore, the display of the model output in spatial and temporal context through the GIS mapping window and the additional time series tool could allow informative results that may be less obvious without the application of these visualization techniques in traditional analysis.

Acknowledgements This research was supported by the National Natural Science Foundation of China (Grant Nos. 51179025 and 50839001). We also acknowledged Prof. Changsheng Chen (University of Massachusetts, Dartmouth) for providing the source code of FVCOM.

References

Atkinson G D, Holliday C R (1977). Tropical cyclone minimum sea-level pressure-maximum sustained wind relationship for the western North Pacific. Monthly Weather Review, 105(4): 421–427

Blumberg A F, Mellor G L (1987). A description of a three-dimensional coastal ocean circulation model. In: Heaps N, ed. Three-Dimensional Coastal Ocean Models 4. Washington D C: American Geophysical Union, 208

Cao Y, Zhu J (2000). Numerical simulation of effects on storm-induced water level after contraction in Qiantang Estuary. Journal of Hangzhou Institute of Applied Engineering, 72: 24–29 (in Chinese)

Castrogiovanni E M, La Loggia G, Noto L V (2005). Design storm prediction and hydrologic modeling using a web-GIS approach on a free-software platform. Atmospheric Research, 77(1–4): 367–377

Chen C, Liu H, Beardsley R C (2003). An unstructured, finite-volume, three dimensional, primitive equation ocean model: application to coastal ocean and estuaries. Journal of Atmospheric and Oceanic Technology, 20(1): 159–186

Chen C, Cowles G, Beardsley R C (2006). An Unstructured Grid, Finite Volume Coastal Ocean Model: FVCOM User Manual. 2nd ed. SMAST/UMASSD Technical Report-06-0602, 19–35

Chen C S, Huang H S, Beardsley R C, Liu H D, Xu Q C, Cowles G (2007). A finite volume numerical approach for coastal ocean circulation studies: comparisons with finite difference models. Journal of Geophysical Research, 772, 112(C03018), doi: 10.1029/2006JC003485

Conner W C, Kraft K H, Harris D L (1957). Empirical methods for forecasting the maximum storm tide due to hurricanes and other tropical storms. Monthly Weather Review, 85(4): 113–116

Dietsche D, Hagen S C, Bacopoulos P (2007). Storm surge simulations for Hurricane Hugo (1989): on the significance of inundation area. Journal of Waterway Port Coastal and Ocean Engineering–ASCE, 133(3): 183–191

Flather R A (2001). Storm surges. In: Steele J H, Thorpe S A, Turekian K K, eds. Encyclopedia of Ocean Sciences. San Diego: Academic Press, 2882–2892

Frank A U (1993). The Use of Geographical Information Systems: the User Interface is the System. In: Medyckyj-Scott D, Hearnshaw H, eds. Human Factors in Geographical Information Systems, London: Belhaven Press, 3–14

Galperin B, Kantha L H, Hassid S, Rosati A (1988). A quasi-equilibrium turbulent energy model for geophysical flows. Journal of the Atmospheric Sciences, 45(1): 55–62

Gemitzi A , Tolikas D (2004). Development of a sharp interface model that simulates coastal aquifer flow with the coupled use of GIS. Hydrogeology Journal, 12(3): 345–356

Gould M D (1993). Two Views of the User Interface. In: Medyckyj-Scott D, Hearnshaw H, eds. Human Factors in Geographical Information Systems. London: Belhaven Press, 101–110

Guo Y K, Zhang J S, Zhang L X, Shen Y M (2009). Computational investigation of typhoon-induced storm surge in Hangzhou Bay. China. Estuarine, Coastal and Shelf Science, 85(4): 530–536

Harris L D (1959). An interim hurricane storm surge forecasting guide. National Hurricane Research Project 32, US Weather Bureau, Washington D C, 23

Holland G J (1980). An analytic model of the wind and pressure profiles in hurricanes. Monthly Weather Review, 108(8): 1212–1218

Hu K, Ding P, Ge J (2007). Modeling of storm surge in the coastal waters of Yangtze Estuary and Hangzhou Bay, China. Journal of Coastal Research, S1(50): 527–533

Huang H, Chen C, Cowles G W, Winant C D, Beardsley R C, Hedstrom K S, Haidvogel D B (2008). FVCOM validation experiments: comparisons with ROMS for three idealized barotropic test problems. Journal of Geophysical Research-Oceans, 113(C07042): 14

Hubbert G D, Holland G J, Leslie L M, Manton M J (1991). A real-time system for forecasting tropical cyclone storm surges. Weather Forecast, 6(1): 86–97

Hubbert G D, McInnes K L (1999). A storm surge inundation model for coastal planning and impact studies. Journal of Coastal Research, 15: 168–185

Jain I, Chittibabu P, Agnihotri N, Dube S K, Sinha P C, Rao A D (2007). Numerical storm surge model for India and Pakistan. Natural Hazards, 42(1): 67–73

Jakobsen F, Madsen H (2004). Comparison and further development of parametric tropical cyclone models for storm surge modeling. Journal of Wind Engineering and Industrial Aerodynamics, 92(5): 375–391

Jelesnianski C P (1966). Numerical computations of storm surge without bottom stress. Monthly Weather Review, 94(6): 379–394

Jelesnianski C P (1967). Numerical computations of storms surges with bottom stress. Monthly Weather Review, 95(11): 740–756

Jelesnianski C P, Chen J, Shaffer W A (1992). SLOSH: Sea, Lake, and Overland Surges From Hurricanes. NOAA Technical Report NWS 48, 77

Kliem N, Nielsen J W, Huess V (2006). Evaluation of a shallow water unstructured mesh model for the North Sea–Baltic Sea. Ocean Model, 15(1–2): 124–136

Large W G, Pond S (1981). Open ocean momentum flux measurements in moderate to strong winds. Journal of Physical Oceanography, 11 (3): 324–336

Li C, Chen C, Guadagnoli G, Georgiou I Y (2008). Geometry induced residual eddies in estuaries with curved channel-observations and modeling studies. Journal of Geophysical Research-Oceans, 113(C01005), doi: 10.1029/2006JC004031

Madsen H, Jakobsen F (2004). Cyclone induced storm surge and flood forecasting in the northern Bay of Bengal. Coastal Engineering, 51 (4): 277–296

McInnes K L, Hubbert G D, Abbs D J, Oliver S E (2002). A numerical modeling study of coastal flooding. Meteorology and Atmospheric Physics, 80(1–4): 217–233

McInnes K L, O'Grady J G, Hubbert G D (2009). Modeling sea level extremes from storm surges and wave setup for climate change assessments in Southern Australia. Journal of Coastal Research, 56 (2): 1005–1009

Mellor G L, Yamada T (1982). Development of a turbulence closure model for geophysical fluid problem. Reviews of Geophysics, 20(4): 851–875

Merkel W H, KaushikaR M, Gorman E (2008). NRCS GeoHydro—a GIS interface for hydrologic modeling. Computers & Geosciences, 34(8): 918–930

Naoum S, Tsanis I K, Fullarton M (2005). A GIS pre-processor for pollutant transport modeling. Environmental Modelling & Software, 20(1): 55–68

Ng S M Y, Wai O W H, Li Y S, Li Z L, Jiang Y W (2009). Integration of a GIS and a complex three-dimensional hydrodynamic, sediment and heavy metal transport numerical model. Advances in Engineering Software, 40(6): 391–401

Peng M, Xie L, Pietrafesa L J (2006a). A numerical study on hurricane induced storm surge and inundation in Charleston, South Carolina. Journal of Geophysical Research-Oceans, 111(C08017): 22

Peng M, Xie L, Pietrafesa L J (2006b). Tropical cyclone induced asymmetry of sea level surge and fall and its presentation in a storm surge model with parametric wind fields. Ocean Model, 14(1–2): 81–101

Powell M D, Houston S H (1998). Surface wind fields of 1995 hurricane Erin, Opal, Luis, Marilyn and Roxanne at landfall. Monthly Weather Review, 126(5): 1259–1273

Resio D T, Westerink J J (2008). Modeling the physics of storm surges. Physics Today, 61(9): 33–38

Smagorinsky J (1963). General circulation experiments with the primitive equations, I: the basic experiment. Monthly Weather Review, 91(3): 99–164

Tsanis I K, Boyle S (2001). A 2D hydrodynamic/pollutant transport GIS model. Advances in Engineering Software, 32(5): 353–361

Tsanis I K, Gad M A (2001). A GIS precipitation method for analysis of storm kinematics. Environmental Modeling & Software, 16(3): 273–281

Wang J Y, Chai F (1989). Nonlinear interaction between astronomical tides and storm surges at Wusong Tidal Station. Chinese Journal of Oceanology and Limnology, 7(2): 135–142

Weisberg R H, Zheng L Y (2006a). A simulation of the hurricane Charley storm surge and its breach of North Captiva Island. Florida Scientist, 69: 152–165

Weisberg R H, Zheng L Y (2006b). Hurricane storm surge simulations for Tampa Bay. Estuaries Coasts, 29(6A): 899–913

Weisberg R H, Zheng L Y (2008). Hurricane storm surge simulations comparing three dimensional with two-dimensional formulations based on an Ivan-like storm over the Tampa Bay, Florida region. Journal of Geophysical Research-Oceans, 113(C1201): 17

Yin B S, Xu Z H, Huang Y, Lin X (2009). Simulating a typhoon storm surge in the East Sea of China using coupled model. Progress in Natural Science, 19(1): 65–71

Zampato L, Umgiesser G, Zecchetto S (2006). Storm surge in the Adriatic Sea: observational and numerical diagnosis of an extreme event. Advances in Geosciences, 7: 371–378

Liang Wang, Ph.D. candidate at the Key State Laboratory of Coastal & Offshore Engineering, Dalian University of Technology, Dalian, China. He was born in 1983, graduated and obtained his B.S. from Chang'an University, Xi'an, China in 2006. He has worked as Master-Doctor combined program graduate student at Dalian University of Technology since from 2006. His research interests involve Environmental Hydraulics as well as Mode of Coupled Application with GIS and Engineering Model. Email: wang.liang200808@gmail.com.

Dr. Xiaodong Zhao, Professor at Dalian University, he obtained his Ph.D., M.S. and B.S. from Shandong University of Science and Technology (SDUT) of China in 2000, 1995 and 1991, respectively. After receiving his M.S., he worked at SDUT, and joined the SDUT as a Lecturer and an Associate Professor, respectively. Currently, he is a Professor at Dalian University. His primary research interests focuse on the areas of Engineering Model coupling with GIS, with special emphasis on modeling of hydrodynamics and geotechnical engineering. Dr. Zhao has published over 50 journal papers. Email: xdong.zhao@gmail.com

Dr. Yongming Shen, Professor at the Dalian University of Technology, China, he obtained his Ph.D., M.S. and B.S. from Chengdu University of Science and Technology, China in 1991, 1988 and 1983, respectively. After receiving his Ph.D., he worked at the Key State Laboratory of Coastal & Offshore Engineering, Dalian University of Technology as a postdoctoral fellow for two years, and then joined the Dalian University of Technology as an Associate Professor. His primary research interests focuse on the areas of Environmental Hydraulics and Computational Hydraulics, with special emphasis on modeling of hydrodynamics, water quality and oil spills for rivers and coastal waters. Dr. Shen has published over 180 journal papers.